

# Numerical simulations and simplified models of nonlinear electron inertial Alfvén waves

R. Rankin and V. T. Tikhonchuk<sup>1</sup>

Department of Physics, University of Alberta, Edmonton, Alberta, Canada

**Abstract.** We describe nonlinear resonance absorption of compressional Alfvén waves in a model magnetosphere. It is shown that the ponderomotive force of excited standing shear Alfvén waves can lead to nonlinear saturation and spatial structuring of field line resonances and that in low-beta plasmas ponderomotive saturation may occur before other nonlinear saturation processes such as the Kelvin-Helmholtz instability. The effects of finite electron inertia are also considered, and it is shown that spatial structuring of field line resonances may occur with scale sizes compatible with those found in discrete auroral arcs. Results are discussed in the context of three-dimensional numerical solutions to the resistive magnetohydrodynamic equations and based on a simplified analytical model of nonlinear resonance absorption.

## 1. Introduction

Ultra low frequency (ULF) waves in the terrestrial magnetosphere [Cummings *et al.*, 1969; Samson, 1972] are often identified as global compressional wave modes trapped inside an inhomogeneous magnetospheric cavity [Kivelson and Southwood, 1985, 1986]. These global modes can excite field line resonances (FLRs) through mode conversion of compressional Alfvén wave energy to shear Alfvén waves (SAWs) on localized resonant magnetic surfaces in the magnetosphere. Mode conversion in the magnetosphere is a three-dimensional process which, in general, requires sophisticated computational models for accurate modeling [Samson and Rankin, 1994; Rankin *et al.*, 1993b] of nonlinear effects. Here we shall discuss nonlinear effects that might be responsible for the saturation of certain FLRs and which can give rise to azimuthal and radial structuring of the wave fields. In the magnetosphere, the SAW excited at the resonance surface constitutes a standing pattern along the magnetic field lines with a node in the magnetic field and an antinode in the velocity field in the equatorial plane. In a warm plasma,  $\beta \approx 1$ , it has been demonstrated that FLRs that have been excited to large amplitude may evolve nonlinearly through the Kelvin-Helmholtz (KH) instability [Rankin *et al.*, 1993b].

We shall consider mode conversion of compressional waves to SAW FLRs on closed geomagnetic field lines close to the Earth, at 8–10  $R_E$  in the equatorial plane.

A primary interest in these FLRs is that they can produce field-aligned currents (FACs) above the auroral ionospheres which are compatible with those found in many discrete auroral arcs, with FACs amounting to several  $\mu\text{A}/\text{m}^2$ . During one half of the wave cycle, an excited FLR will have a large upward FAC in the latitudinal center of the waveform, with two regions of smaller-amplitude, downward directed FACs on either side [Greenwald and Walker, 1980]. Observational features of these FLRs show a 180° phase decrease with increasing latitude, as a result of spatial gradients in the Alfvén speed toward the Earth. For 1- to 4-mHz waves, FLRs also exhibit periodic restructuring over timescales of several minutes. For example, Samson *et al.* [1996b], using meridian scanning photometer and magnetometer data, identified a 2.6- to 2.8-mHz FLR in the evening sector which was observed for a number of hours. The H $\beta$  emissions from precipitating protons placed the location of this FLR on geomagnetic field lines threading the inner edge of the plasma sheet. The FLR was observed to form large-scale vortex structures during various stages of its evolution. Vortex formation in FLRs may occur if the velocity field of the excited SAW can be driven to large amplitude (roughly 100 km/s over a scale size of 0.1  $R_E$  in the equatorial plane of the magnetosphere), which is possible, provided dissipation and nonlinear saturation processes are unimportant. In the equatorial plane, the velocity fields of FLRs might then allow Kelvin-Helmholtz (KH) instabilities to form. This offers an explanation for the large-scale vortex structures (with scale sizes of hundreds of kilometers) given by Samson *et al.* [1996b] and in other auroral arcs [Rankin *et al.*, 1993b; Samson and Rankin, 1994].

Possible external sources that can excite FLRs include pressure pulses from the solar wind [Southwood and Hughes, 1983; Yumoto, 1988; Allan and Poulter,

<sup>1</sup>On leave from the P. N. Lebedev Physics Institute, Russian Academy of Sciences, Moscow.

1992; Lee and Wei, 1993], and many measurements of ULF standing wave FLRs in the terrestrial magnetosphere have been made, from the early observations of Cummings *et al.* [1969] and Samson [1972], to a variety of more recent observations that use HF radar [Ruohoniemi *et al.*, 1991; Samson *et al.*, 1992; Walker *et al.*, 1992; Fenrich *et al.*, 1995], ground-based magnetometers [Samson *et al.*, 1992; Ziesolleck and McDiarmid, 1994], and optical techniques [Samson *et al.*, 1992; Samson *et al.*, 1991; Xu *et al.*, 1993; Samson *et al.*, 1996a]. These observations indicate that in the equatorial magnetosphere, FLRs might have radial scale sizes of one tenth of an Earth radius or less. When mapped along dipole field lines to the ionospheres, these scale sizes become comparable to those found in many 10-km-scale discrete auroral arcs. Indeed, substantial observational evidence now suggests that many auroral arcs are associated with FLR structures, as discussed, for example, by Samson *et al.* [1996a, b].

A further interest in FLRs is that they can lead to large parallel electric fields, of the order of 1 V/m, above the ionospheres, particularly at altitudes in the vicinity of  $1 R_E$ , where inverted-V electron precipitation is commonly observed [Weimer and Gurnett, 1993]. As discussed by Goertz [1984], Wei *et al.* [1994] and Streltsov and Lotko [1995], large parallel electric fields in FLRs can be generated through electron inertia effects after the wave fields have narrowed to a number (typically 6 or 7) of electron inertial lengths. With finite electron inertia, the wave fields are limited in amplitude by dispersive effects, and a FLR will normally consist of a spatial wave train that has a number of electric field peaks as one moves equatorward of the resonance position. These features have previously been attributed to electrostatic shocks [Mozer, 1981], but they may be more simply explained as the dispersive effects of FLRs. A recent study by Samson *et al.* [1996a], who used the Canadian Auroral Network for the OPEN Program Unified Study (CANOPUS) array of magnetometers, meridian scanning photometers, and a digital all-sky imager, showed strong evidence of auroral arcs formed by FLRs. They also observed spatial structure within FLRs which had latitudinal scale sizes of 10-15 km that are consistent with dispersive FLRs. Meridian scans of the all-sky imager data showed that the arcs had an inverted-V structure, with maximum energies ranging from several hundred eV to 1 or 2 keV.

Within the framework of linear analysis, a number of important and ground-breaking theories have been developed to explain the coupling that occurs between compressional MHD wave energy and standing SAW FLRs [Kivelson and Southwood, 1985, 1986; Chen and Hawegawa, 1974; Southwood, 1974; Zhu and Kivelson, 1988; Lee and Lysak, 1989], and a clear understanding of the linear behavior of FLRs has emerged. The wave fields in FLRs can, however, become quite large, and clearly at some point nonlinear effects should be considered. One key question is whether nonlinear effects still permit large amplitude waves to form and whether the nonlinear evolution of FLRs is in agreement with observations. In previous work, we discussed

a mechanism of SAW nonlinearity which arises due to the ponderomotive force of the waves. This mechanism is especially important in the case of standing SAWs and may result in ion acceleration [Allan, 1993; Li and Temerin, 1993], wave profile steepening, field-aligned spatial harmonic generation [Rankin *et al.*, 1994], and chaotic-like temporal behavior of the amplitudes of excited waves [Tikhonchuk *et al.*, 1995]. Our theoretical findings correlate well with large density depletions (of order one) that have been observed in association with SAWs [Boehm *et al.*, 1990].

Using a model in which a SAW is excited by a driver field in a homogeneous plasma, it was demonstrated by Rankin *et al.*, [1994] and Tikhonchuk *et al.*, [1995] that the ponderomotive force leads to nonlinear detuning of the standing SAW eigenmode from the driver, and ultimately the excited SAW can saturate by decoupling itself from the driver. These results suggest that the ponderomotive force of standing SAWs might also be an effective mechanism of nonlinear saturation of FLRs [Rankin *et al.*, 1995] driven by global compressional modes. The ponderomotive saturation mechanism may effectively compete with the Kelvin-Helmholtz instability or precede and modify its temporal development.

In this paper we derive a simplified set of equations that can be used to describe ponderomotive effects in dispersive field line resonances. We derive analytical expressions for the amplitude and time of ponderomotive saturation of field line resonances, describe observational features of our models, and compare them with three-dimensional (3-D) fully nonlinear MHD simulations in a simplified 3-D Cartesian geometry.

## 2. Basic Equations

We describe FLRs in a global magnetospheric system for which the governing equations consist of the full set of resistive MHD equations with the inclusion of electron inertia in the generalized Ohms law.

$$\frac{\partial \rho}{\partial t} + \nabla \cdot (\rho \mathbf{V}) = 0 \quad (1)$$

$$\rho \left( \frac{\partial}{\partial t} + \mathbf{V} \cdot \nabla \right) \mathbf{V} = -\nabla P + \mathbf{J} \times \mathbf{B} + \nu \nabla^2 \mathbf{V} \quad (2)$$

$$\nabla \times \mathbf{E} = -\frac{\partial \mathbf{B}}{\partial t} \quad (3)$$

$$\nabla \times \mathbf{B} = \mu_0 \mathbf{J} \quad (4)$$

$$\mathbf{E} + \mathbf{V} \times \mathbf{B} = \eta \mathbf{J} + \frac{m_e}{ne^2} \frac{\partial \mathbf{J}}{\partial t} \quad (5)$$

Here  $\mathbf{B}$  is the magnetic field,  $\mathbf{E}$  is the electric field,  $\mathbf{J}$  is the electric current density,  $\rho$  is the density, and  $P$  is the pressure. The coefficients  $\nu$  and  $\eta$  stand for the plasma viscosity and resistivity, respectively. In the Ohms law, equation (5), the electron inertial term is represented by the second term on the right-hand side, while the first term on the right describes the effects of magnetic

field diffusion. We have ignored the electron pressure term in Ohms law, although under certain conditions it may become important in the vicinity of the equatorial plane. Electron inertial and ponderomotive effects become appreciable at low altitudes 1-2  $R_E$ , where large parallel electric fields are commonly observed and where the plasma  $\beta$  is significantly less than  $m_e/m_i$ . We have also ignored the nonlinear electron inertia term in Ohms law and, because we are considering only ULF waves, have omitted the Hall term. In presenting various forms of solution to the above equations, we note that the electric field can be eliminated by substituting Ohm's law (equation (5)) into the Faraday equation (3), and, correspondingly, the current density can be eliminated from the momentum equation (2) using Ampere's law (equation (4)). This leads to a set of equations involving the eight unknowns  $\mathbf{V}$ ,  $\mathbf{B}$ ,  $\rho$ , and  $P$ .

In the following sections we present solutions to the MHD equations in a 3-D Cartesian geometry [Rankin *et al.*, 1993a; Wei *et al.*, 1994]. In this model, coordinate  $x$  is radial,  $y$  is azimuthal, and  $z$  is field aligned. The ionospheres are at opposite ends of straight magnetic field lines and are bounded on the left by the magnetopause and on the right by a boundary that is earthward of the turning point of compressional Alfvén waves. This so-called box model is an approximation that gives a reasonable description of the behavior of radially localized wave modes in the near-Earth magnetosphere. The justification for this model is provided by the fact that the perpendicular scale of the wave structures being examined is much less than their field-aligned extent. Further justification is provided by the fact that the eigenfunctions and eigenfrequencies of shear Alfvén and compressional waves are primarily influenced by the density and magnetic field in the region of the equatorial plane, which is correctly represented in our model. However, the box model does not account for the geometrical variation of perpendicular scales along the geomagnetic field. Therefore when we turn to a discussion of inertial effects, we choose a perpendicular scale that is relevant to the ionospheric end of the field line, where inertial scales become important. The box model magnetosphere also neglects magnetic curvature. However, the effects of curvature are negligible for the low- $m$  wave modes discussed in this paper.

### 3. Slowly Varying Envelope Equations

In developing a simplified model of FLRs, we shall examine the nonlinear evolution of coupled compressional and SAWs in an inhomogeneous low-beta plasma by constructing a perturbation expansion of the fields in equations (1)-(5) of the form  $A = A_0 + \epsilon A^{(1)} + \epsilon^2 A^{(2)} + \epsilon^3 A^{(3)}$ , where  $\epsilon$  is a small expansion parameter which is proportional to the amplitude of the excited Alfvén wave or driver. In the linear approximation, to order  $\epsilon$ , we can neglect the effect of plasma pressure by assuming that  $\beta \equiv 2\mu_0 P_0/B_0^2 \ll 1$ . We shall also assume that dissipation effects are small and account for them in the linear approximation. Defining the plasma dis-

placement  $\mathbf{V} = \partial\xi/\partial t$ , the  $x$  component of the equation of plasma motion provides a relationship between  $\xi_x$  and  $b_x$

$$\left( \frac{1}{V_A^2} \frac{\partial^2}{\partial t^2} - \frac{\lambda_e^2}{V_A^2} \nabla^2 \frac{\partial^2}{\partial t^2} - \frac{\nu/\rho_0 + \eta/\mu_0}{V_A^2} \nabla^2 \frac{\partial}{\partial t} - \frac{\partial^2}{\partial x^2} \right) \xi_x = -\frac{1}{B_0} \frac{\partial b_x}{\partial x}, \quad (6)$$

where  $V_A(x) = \sqrt{B_0^2/\mu_0\rho_0}$  is the local Alfvén velocity. Similarly, we can also write the  $y$  component of the plasma displacement in terms of  $b_x$ :

$$\left( \frac{1}{V_A^2} \frac{\partial^2}{\partial t^2} - \frac{\lambda_e^2}{V_A^2} \nabla^2 \frac{\partial^2}{\partial t^2} - \frac{\nu/\rho_0 + \eta/\mu_0}{V_A^2} \nabla^2 \frac{\partial}{\partial t} - \frac{\partial^2}{\partial x^2} \right) \xi_y = -\frac{1}{B_0} \frac{\partial b_x}{\partial y}. \quad (7)$$

Making use of Faraday's law and taking the divergence of the equation of plasma motion perpendicular to the ambient magnetic field, we also obtain a relationship between  $b_x$  and  $\xi_x$ ,

$$\left( \frac{1}{V_A^2} \frac{\partial^2}{\partial t^2} - \frac{\lambda_e^2}{V_A^2} \nabla^2 \frac{\partial^2}{\partial t^2} - \frac{\nu/\rho_0 + \eta/\mu_0}{V_A^2} \nabla^2 \frac{\partial}{\partial t} - \frac{\partial^2}{\partial x^2} - \nabla_{\perp}^2 \right) b_x = B_0 \frac{\partial^2 \xi_x}{\partial t^2} \frac{d}{dx} \frac{1}{V_A}, \quad (8)$$

where  $\nabla_{\perp}$  stands for the gradient perpendicular to the ambient magnetic field.

In a homogeneous plasma the linear dispersion relations for SAWs and compressional Alfvén waves follow from equations (6)-(8) if we assume variations of the fields of the form  $\exp i(\omega t - k_x x - k_y y - k_z z)$ :

$$\omega^2 = \frac{k_z^2 V_A^2}{1 + k^2 \lambda_e^2}, \quad \omega^2 = \frac{k^2 V_A^2}{1 + k^2 \lambda_e^2}. \quad (9)$$

The second expression describes the compressional wave, and although the dispersion relation of this mode is modified by electron inertia, it can easily be shown that the SAW (the first expression in equation (9)) is more significantly affected by the term  $1 + k^2 \lambda_e^2$  in the denominator. In an inhomogeneous plasma, we may regard  $k_x$  as a function of  $x$  and note that as the wave fields of the FLR narrow with time,  $k_x$  may become large enough to move the resonance position equatorward. More significant, perhaps, is the development of a parallel electric field  $E_z = -i\omega \lambda_e^2 \mu_0 J_z$ , which, again, only becomes significant after the wave fields have narrowed and, correspondingly, the parallel current has become very large. Note that the parallel current is entirely due to the magnetic field of the SAW.

Continuing with our derivation, we now consider a plasma that is subjected to an external source of frequency  $\omega$  which excites SAWs in the vicinity of the critical layer,  $x = x_c$ , where the resonance condition,  $V_A^2(x_c) = \omega^2/k_x^2$ , is satisfied. For low- $m$  (long azimuthal wavelengths) modes characteristic of many FLRs in the magnetosphere, it is known that the most significant enhancement of the fields is experienced by the SAW magnetic field component,  $b_y$ , and displacement,  $\xi_y$ .

Keeping this in mind, we shall proceed with our study of the nonlinear temporal evolution of FLRs by considering standing waves along the ambient magnetic field lines.

We can simplify equations (6)-(8) by taking a Fourier transform in the homogeneous direction  $y$  and by using a slowly varying envelope approximation in time. This implies that the  $z$  component of the magnetic field and the  $x$  and  $y$  components of the displacement can be represented as  $A(x, y, z, t) = \text{Re}[A(x, t) \exp(i\omega t - ik_y y)] \sin(k_z z)$ , where the envelope approximation in time means that the complex amplitude  $A(x, t)$  is assumed to change in time on a scale that is much longer than the driver period. The explicit coordinate dependence in our equations arises from the inhomogeneity of the reference state,  $V_A^2(x)$ , and since coupling between the compressional and SAW modes is strongest in a narrow region surrounding the resonance point,  $x_c$ , we can approximate the Alfvén velocity there by a linear function:

$$\frac{1}{V_A^2} \approx \frac{k_z^2}{\omega^2} \left( 1 - \frac{x - x_c}{L} + \frac{\delta\rho}{\rho_0} \right). \quad (10)$$

For the purposes of the nonlinear description of the resonance, we have retained the ponderomotive density perturbation,  $\delta\rho$ , in this expansion. To derive an equation for the density perturbations, we note that the ponderomotive force of a SAW excites plasma motion along magnetic field lines and drives corresponding nonlinear density perturbations. The equation for the density perturbations follows from the longitudinal  $z$  component of the equation of motion in the equation (2), together with the continuity equation, equation (1). Nonlinear effects appear in second order, and it is straightforward to derive an equation which describes a slow magnetosonic plasma wave (SMW) that is excited by the ponderomotive force of SAWs:

$$\left( \frac{\partial^2}{\partial t^2} + \Gamma_S \frac{\partial}{\partial t} - C_S^2 \frac{\partial^2}{\partial z^2} \right) \frac{\delta\rho}{\rho_0} = \frac{\partial^2}{\partial z^2} \frac{b_y^2}{2\mu_0}. \quad (11)$$

Here  $C_S = \sqrt{\delta P / \delta\rho}$  is the ion acoustic velocity and  $\Gamma_S = -(\nu/\rho_0)\nabla^2$  is an operator which describes spatial damping of the ion acoustic wave. Because of the dependence on  $b_y$ , the driven SMW remains localized to the resonance region where the SAW magnetic field is large. Recognizing the very different wave periods of the SMW and the SAW, we can average the right-hand side of equation (11) over the fast timescale  $\omega^{-1}$  of the SAW, and find that the ponderomotive force has a slowly varying in time component which drives second spatial harmonic,  $(k_y = 0, 2k_z)$ , density perturbations,  $\delta\rho/\rho_0 = n \cos(2k_z z)$ . The amplitude  $n(x, t)$  of these density perturbations satisfies the driven ion acoustic wave equation

$$\left( \frac{\partial^2}{\partial t^2} + \Gamma_S \frac{\partial}{\partial t} + 4k_z^2 C_S^2 \right) n = -\frac{\omega^2}{2B_0^2} b_y^2. \quad (12)$$

Using equation (10) and the approximate relations,  $b_{x,y} = k_z B_0 \xi_{x,y}$ , we complete our system of equations by writing equations (6)-(8) in the form

$$\left( \frac{2i}{\omega} \frac{\partial}{\partial t} + \lambda_e^2 \frac{\partial^2}{\partial x^2} + \frac{i}{\omega} \Gamma_A + \frac{x-x_c}{L} + \frac{1}{2}n + \frac{k_y^2}{k_z^2} - \frac{1}{k_z^2} \frac{\partial^2}{\partial x^2} \right) b_z = -\frac{1}{k_z L} b_x, \quad (13)$$

$$\left( \frac{2i}{\omega} \frac{\partial}{\partial t} + \lambda_e^2 \frac{\partial^2}{\partial x^2} + \frac{i}{\omega} \Gamma_A + \frac{x-x_c}{L} + \frac{1}{2}n \right) b_x = -\frac{1}{k_z} \frac{\partial b_x}{\partial x}, \quad (14)$$

$$\left( \frac{2i}{\omega} \frac{\partial}{\partial t} + \lambda_e^2 \frac{\partial^2}{\partial x^2} + \frac{i}{\omega} \Gamma_A + \frac{x-x_c}{L} + \frac{1}{2}n \right) b_y = i \frac{k_y}{k_x} b_z. \quad (15)$$

Here the operator  $\Gamma_A = -(\eta/\mu_0 + \nu/\rho_0)\nabla^2$  describes resistive or viscous Alfvén wave damping, and the dispersion relation for SAWs was expanded around the resonance point  $x_c$  according to

$$1 + k_0^2 \lambda_e^2 - \frac{k_z^2 V_A^2(x)}{\omega^2} \approx \frac{k_z^2 V_A^2(x_c)}{\omega^2} \left( 1 - \frac{V_A^2(x)}{V_A^2(x_c)} \right), \quad (16)$$

where  $k_0^2 = k_y^2 + k_z^2$ . Note that in equation (16), the right-hand side vanishes only at  $x = x_c$ , and away from the resonance position a spatial frequency mismatch  $\Delta\omega(x) = \omega(x_c - x)/2L$  develops which is responsible for phase mixing.

#### 4. Model Equations for Coupled Standing Shear Alfvén and Slow Mode Waves

Equations (13)-(15) describe three Alfvén eigenmodes in an inhomogeneous plasma: one compressional mode (the first equation) and two shear ones. The first two equations are coupled due to the plasma inhomogeneity; the third mode is attached only in a three-dimensional geometry, i.e., provided  $k_y \neq 0$ . This last case is of interest for the study of FLRs because for low- $m$  modes, only the  $y$  component of the magnetic field experiences a strong enhancement at the resonance position. One should also note that when damping and electron inertia are negligible, shear components excited on particular field lines do not easily couple to neighboring field lines ( $x$  is simply a parameter), and thus SAWs excited on different field lines will evolve more or less independently.

It was shown by Rankin *et al.* [1994] that small-amplitude SAWs can excite large ponderomotive density perturbations which nonlinearly modify the SAW because of a spatial modulation of the Alfvén velocity profile (equation (10)). It is evident from equations (13)-(15) that for the situation considered here, the density perturbations lead to a nonlinear shift of the resonant layer position,  $x_c \rightarrow x_c - nL/2$ . In the model of homogeneous plasmas [Tikhonchuk *et al.*, 1995] this effect is interpreted as nonlinear frequency detuning. On

a particular magnetic field line, it leads to local nonlinear saturation of shear Alfvén waves that are driven by an external monochromatic source. We shall see that similar effects occur in the case of inhomogeneous plasmas.

We shall consider here the case of relatively weak density perturbations for which the nonlinear shift of the critical layer is much less than the distance between  $x_c$  and the turning point,  $x_t$ , of the compressional Alfvén wave,  $x_c - x_t = Lk_y^2/k_z^2 \gg |n|L$ . We shall also neglect damping of the compressional Alfvén wave for the sake of simplicity. With these assumptions, the density perturbation and time derivative terms can be neglected in equations (13) and (14), which then reduce to the equation

$$\frac{\partial^2 b_z}{\partial x^2} - \frac{1}{x - x_c} \frac{\partial b_z}{\partial x} - \left( k_y^2 + k_z^2 \frac{x - x_c}{L} \right) b_z = 0, \quad (17)$$

studied in the theory of linear resonance absorption [Speziale and Catto, 1977]. According to Speziale and Catto [1977], the field  $b_z$  contains forward,  $b_z^+$ , and backward,  $b_z^-$ , propagating waves in the transparent region,  $x < x_t$ , and becomes evanescent in the forbidden region,  $x > x_t$ . In the vicinity of the critical layer,  $x = x_c$ ,  $b_z$  is approximately constant,  $b_z(x) \approx b_c[1 + (q/2)\zeta^2 \ln \zeta]$ , with only a logarithmic divergence of its second derivative. Here  $q = (k_z L)^{2/3} k_y^2/k_z^2$  and  $\zeta = (x - x_c)k_z^{2/3}/L^{1/3}$  are the standard notations used in resonance absorption theory, and the amplitude of the magnetic field in the critical layer,  $b_z(x_c) = b_c$ , can be related to the incident compressional Alfvén wave energy flux,  $S_0 = E_y^+ b_z^+ / 2\mu_0$ , through the energy conservation condition:

$$\frac{\pi}{2} q (k_z L)^{1/3} \frac{\omega}{k_z} \frac{b_c^2}{2\mu_0} = AS_0. \quad (18)$$

The absorption coefficient  $A(q)$ , which is a function of the parameter  $q$  only, has been calculated numerically by Forslund *et al.* [1975]. For practical applications the following simple asymptotical expressions may be useful:  $A(q \ll 1) \approx 2.6q(1 - 1.7q)$ ,  $A(q \gg 1) \approx 2 \exp(-\frac{4}{3}q^{3/2}) - \exp(-\frac{8}{3}q^{3/2})$  as discussed by Speziale and Catto [1977]. The maximum absorption  $A \approx 0.5$  occurs for  $q \approx 0.5$ .

From the discussion above, it can be seen that in the vicinity of the resonant layer the right-hand side of equation (15) can be treated as an approximately constant source,  $ib_c k_y/k_z$ , which drives the shear component  $b_y$ . In the absence of the electron inertia terms, the equations for  $b_y$  and for the density perturbation, Equation (12), are of the same form as the equations for nonlinear driven SAWs that arise in homogeneous plasmas [cf. Tikhonchuk *et al.*, 1995, equation (18)]. Writing our inhomogeneous plasma equations in the same form as Tikhonchuk *et al.* [1995], we find

$$\dot{b} - \frac{i}{2}\omega\lambda_e^2 \frac{\partial^2 b}{\partial x^2} + \Gamma_a b = -i(\Delta\omega - \frac{1}{4}\omega n) b + \frac{1}{2}R\omega, \quad (19a)$$

$$\ddot{n} + 2\Gamma_s \dot{n} + \Omega^2 n = -\frac{1}{2}\omega^2 |b|^2, \quad (19b)$$

where  $b(t) = b_y/B_0$ . Here  $R = k_y b_c/k_z B_0$  is the dimensionless strength of the driver, and  $\Delta\omega(x)$  is the spatial linear frequency detuning parameter defined earlier. In passing, we will note that when electron pressure is important, the dispersion term in equation (19) can be replaced by  $+i\omega/2\rho_s^2 \partial^2 b/\partial x^2$ , where  $\rho_s = \lambda_e V_{Te}/V_A$  and  $V_{Te}$  is the electron thermal speed. This dispersion is of opposite sign to electron inertia and may become important in the hot plasma region near to the equatorial magnetosphere. A detailed analysis of the competing effects requires a more sophisticated model that includes field-aligned variations of the ambient parameters. Here we restrict our discussion to effects that might dominate near to the auroral ionosphere.

Equations (19a) and (19b) describe the nonlinear interaction between two parametrically coupled oscillators: a SAW and a SMW. The SAW oscillator experiences a nonlinear frequency shift,  $\omega n/4$ , that is directly proportional to the amplitude of the SMW, and the SMW oscillator is driven by a ponderomotive force that depends on the intensity of the SAW. This system (equations (19a) and (19b)) has two characteristic timescales: One timescale is related to the magnetosound period or plasma  $\beta$ , and the other is associated with the timescale for SAW nonlinear effects. In the following section we discuss the behavior of the nonlinear model of FLRs described by equations (19a) and (19b).

## 5. Nonlinear Saturation Mechanisms and Timescales

In this section, we shall discuss saturation mechanisms and characteristic timescales associated with the model equations derived in section 4. First of all, we note that equations (19a) and (19b) possess conservation properties. Multiplying equation (19a) by  $b^*$  and adding it to its conjugate, we obtain after some rearrangement,

$$\frac{d}{dt} |b|^2 + 2\Gamma_a |b|^2 + \omega \frac{\partial}{\partial x} \left( \lambda_e^2 \text{Im} b^* \frac{\partial b}{\partial x} \right) = \omega R \text{Re}(b). \quad (20)$$

On the left-hand side of this equation, the second term represents spatial damping, the third term results from the poynting flux of the electron inertia SAW, and the right-hand side is a source term due to the compressional driver. Note that the density perturbations in equations (19a) and (19b) do not affect the energy of the SAW. The density perturbation produces a temporal nonlinear frequency shift that can turn on and off the coupling, but there is no net transfer of energy between the driven SMW and the SAW.

First of all, we review the linear predictions of our model by ignoring the density perturbation in equation (19a). Neglecting dissipation and electron inertia for the moment, the linear solution for  $b$  reads

$$b = R \frac{\omega}{\Delta\omega} \sin\left(\frac{1}{2}\Delta\omega t\right) \exp\left(-\frac{i}{2}\Delta\omega t\right). \quad (21)$$

Using the above expression, it can be seen that in the vicinity of the resonance position, within the thin layer  $\delta x \approx 4\pi L/\omega t$  (where the linear mismatch  $\Delta\omega$  is small), the excited SAW experiences secular growth,  $b = R\omega t/2$ . This growth corresponds to absorption of the energy of the compressional Alfvén wave. Indeed, the shear mode energy  $W = \int_{-\infty}^{\infty} dx |b_y|^2 / 4\mu_0$  grows linearly with time and, according to equation (18), is associated with an amount of compressional wave absorption  $W = AS_0 t$ .

In the absence of nonlinear effects, spatial wave damping and group velocity effects of electron inertia in equations (19a) and (19b) will eventually lead to saturation of  $b$  at the resonance layer. Considering first of all dissipative effects, it can be shown that linear dissipative saturation will occur in the case of a weak driver satisfying  $R < 8(\beta\gamma)^{1/2}(\Gamma_a/\omega)^{3/2}$ , where  $\gamma$  is the adiabatic index. From equations (19a) and (19b), the level of dissipative saturation can then be found by comparing the effective spatial damping,  $\Gamma_A \sim (\eta/\mu_0 + \nu/\rho_0)/(\delta x)^2$ , with the characteristic scale width of the resonance  $\omega\delta x/L$ , at saturation. The timescale of dissipative saturation,  $t_{ds}$ , and the amplitude of the SAW magnetic field at saturation are given by

$$t_{ds} \approx 4\pi \left(\frac{L}{\omega}\right)^{2/3} \left(\frac{\eta}{\mu_0} + \frac{\nu}{\rho_0}\right)^{-1/3}, \quad b_{y,ds} \approx \frac{1}{2} B_0 R \omega t_{ds}. \quad (22)$$

In the case of ULF waves in the magnetosphere, viscosity and resistivity are likely unimportant, and the coefficient  $\eta/\mu_0$  in equation (22) can be replaced by, for example, the corresponding term due to ionospheric damping.

In the linear regime where dissipation and/or ionospheric damping is negligible, electron inertia will lead to saturation of the wave fields of the FLR. This occurs as a result of the dispersive properties of electron inertia SAWs which can propagate energy out of the resonant layer at the perpendicular group velocity. In this case, the timescale for saturation, and the scale size of structure within the resonance layer at saturation, can be estimated from a comparison of the order of magnitude of the second and last terms in equations (19a) and (19b), again assuming that the resonance layer is of thickness  $\delta x$  at the time of saturation. The amplitude, time of saturation, and thickness of the resonant layer at saturation are given by

$$\begin{aligned} t_{eis} &\approx \frac{2}{\omega} \left(\frac{L}{\lambda_e}\right)^{2/3}, \\ b_{y,eis} &\approx \frac{1}{2} B_0 R \omega t_{eis}, \\ \delta x_{eis} &\approx (L\lambda_e^2)^{1/3}. \end{aligned} \quad (23)$$

In the situation where the scale length of the Alfvén speed profile is of the order of hundreds of electron inertial lengths, the above expressions predict that structure within the resonance will have a spatial scale of the order of several electron inertial lengths. This is consistent with many observations of auroral arcs [Borovsky, 1993].

If dissipation and electron inertia effects are small, the estimated levels of saturation of the FLR defined by equations (22) and (23) become irrelevant, and nonlinear ponderomotive effects should be considered. For a weak driver and/or a warm plasma characterized by the inequality  $R < (8\beta\gamma)^{5/4}$ , the density perturbation (equations (19a) and (19b)) responds adiabatically, and we find that periodic pulsations of the amplitude of the SAW occur. These pulsations are characterized by the following parameters:

$$\begin{aligned} b_{y,\max} &= 32^{1/3} (R\beta\gamma)^{1/3} B_0, \\ |n|_{\max} &= 16^{1/3} (R^2/\beta\gamma)^{1/3}, \\ t_p &= 15.4\omega^{-1} (\beta\gamma/R^2)^{1/3}. \end{aligned} \quad (24)$$

where  $b_{y,\max}$  is the maximum amplitude of the magnetic field at the resonance layer,  $|n|_{\max}$  is a parameter that gives an estimate of the maximum amplitude of the ponderomotive density perturbations in the resonance layer, and  $t_p$  is the period of nonlinear SAW pulsations. The numerical factor in the equation for  $t_p$  comes from the numerical approximation of an integral. It can be shown also that the width of the region of nonlinear saturation of the FLR corresponds to a small amount of frequency detuning,  $|\delta\omega| < 0.4k_z C_S R^{2/3}/(\beta\gamma)^{5/6}$ , and is localized to a small region  $\delta x < L(\beta\gamma R^2)^{1/3}$  surrounding the resonance layer.

In the opposite limit of a strong driver and/or a colder plasma satisfying  $R > (8\beta\gamma)^{5/4}$ , there are no real oscillations of the density perturbation over the time of nonlinear saturation, and the density is found to be secularly growing. In this limit, we can neglect the term  $\Omega^2 n$  in the second equation of system (22). Saturation of the SAW amplitude occurs when the nonlinear term in the first equation of system (22) becomes of the same order of magnitude as the driver. In this case, the SAW magnetic field component is found to saturate according to

$$b_{y,\max} = 2B_0 R^{3/5}, \quad t_{\text{sat}} = 6\omega^{-1} R^{-2/5}, \quad (25)$$

where  $b_{y,\max}$  is the saturation amplitude of the SAW and  $t_{\text{sat}}$  is the time of nonlinear saturation. In this case, the induced nonlinear dephasing between the driver and the excited SAW at the resonance position leads to burst-like chaotic pulsations around the level  $b_{y,\max}$ . These pulsations are due to the fact that the SAW can only gain energy from the compressional driver during intervals for which the phase slip between the waves is not changing rapidly. In the strongly driven cold plasma case, the ponderomotive force in the resonant layer can easily excite density perturbations comparable to the background density. The thickness of the nonlinear layer in that case does not depend on the driver strength.

In discussing linear and nonlinear saturation timescales, it is interesting to note that the regime of ponderomotive saturation defined by equation (25) will easily dominate electron inertia effects provided the driver satisfies the inequality  $R > (L/\lambda_e)^{-5/3}$ . Electron inertia effects will then manifest as a secondary process in the nonlinear evolution of FLRs. We should also

mention here that ponderomotive SAW amplitude saturation prevents further energy absorption of the compressional Alfvén wave. This may affect the magnitude of the driver field  $b_e$  (assumed constant in our model) at the resonance layer, and a self-consistent analysis of equations (12) and (13)-(15) is then required to include the effects of compressional wave amplitude depletion at the time of resonance saturation. However, this is better addressed by solving the full system of equations defined by equations (1)-(5). Nonlinear saturation of the acoustic waves might also be affected by Landau damping. This can possibly lead to high-energy electron bursts that are often seen near the polar ionospheres. Landau damping requires a kinetic treatment for ions and is outside the scope of the MHD formalism used in the present study.

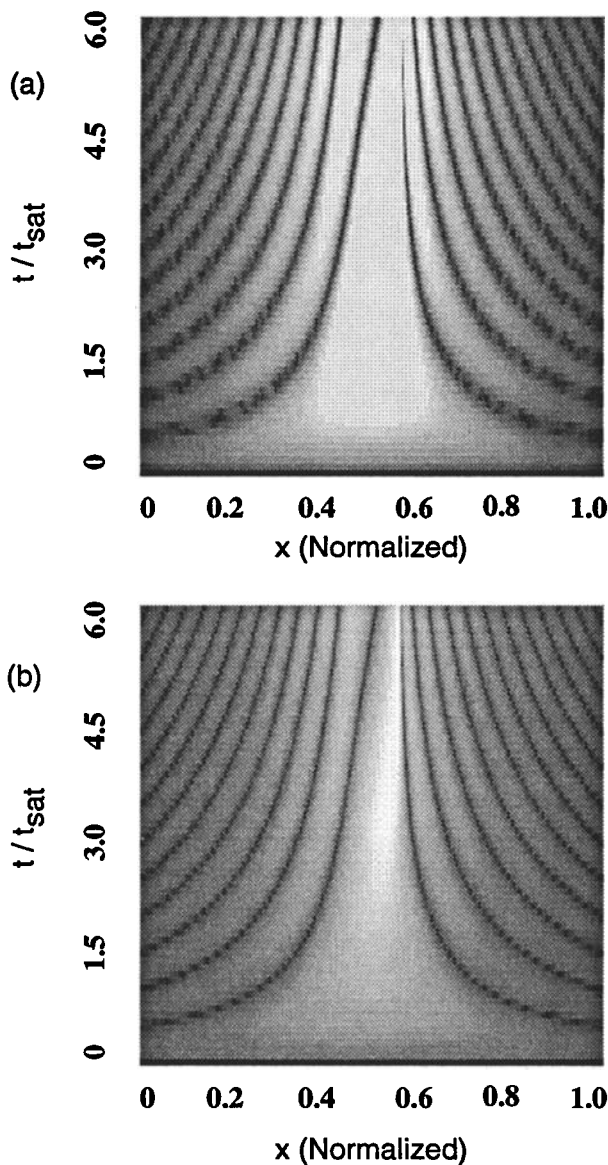


**Figure 1.** The temporal behavior of the amplitude of the (a) magnetic field and (b) density perturbation obtained from the numerical solution to equations (19a) and (19b). Parameters correspond to  $Q = 4.25$  and  $R = 1.32 \times 10^{-4}$ . The electron inertia length is set to zero.

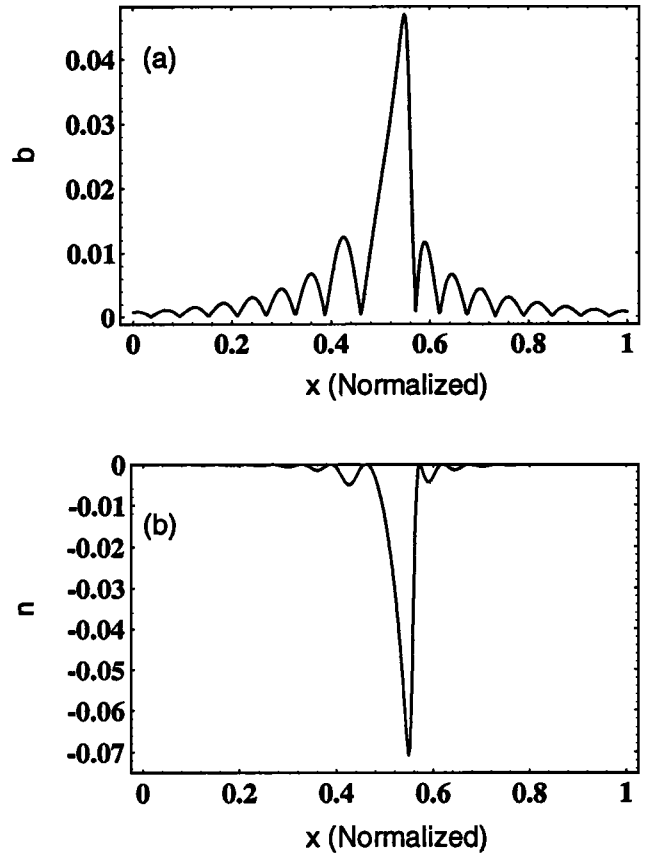


**Figure 2.** The amplitude of the (a) magnetic field and (b) density perturbation as a function of  $x$  obtained from the numerical solution to equations (19a) and (19b). Results are shown at a time corresponding to  $t = 4t_{\text{sat}}$ . Parameters correspond to  $Q = 4.25$  and  $R = 1.32 \times 10^{-4}$ . The electron inertia length is set to zero.

## 6. Numerical Analysis of Simplified Nonlinear Model of FLRs

In this section, we shall examine some of the predictions of our simplified nonlinear models of FLRs that will later be compared with numerical solutions of the fully nonlinear three-dimensional (3-D) MHD equations [Rankin *et al.*, 1993b]. As mentioned by Tikhonchuk *et al.* [1995], it is convenient to define a nonlinear parameter  $Q = \Omega t_{\text{sat}}$ , where  $\Omega = 2k_z C_s$  is the frequency of the driven acoustic wave in equations (19a) and (19b), and  $t_{\text{sat}}$  is a convenient timescale for nonlinear effects, as defined by equation (25). Crudely speaking, very strong nonlinear behavior corresponds to  $Q \lesssim 1$ , whereas  $Q > 1$  results in increasingly milder nonlinear behavior. As discussed above, different temporal behavior of the excited SAW and ponderomotive density perturbation is predicted for the weakly and strongly nonlinear cases, respectively.

As an example, we show in Figures 1-3 results of the numerical solution to equations (19a) and (19b) for  $Q = 4.25$  and  $R = 1.32 \times 10^{-4}$ . Figure 1a is a grey scale plot showing the excited magnetic field  $b$  as a function of  $x$  and time, with the time unit normal-

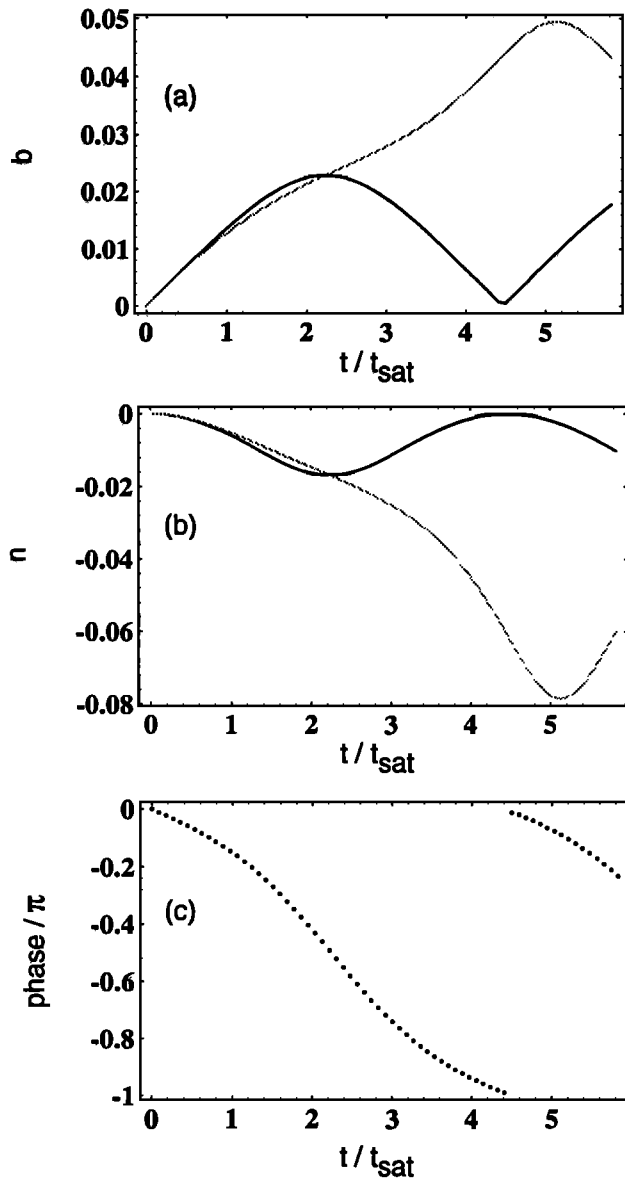


Figure 3. Temporal behavior of (a) magnetic field amplitude, (b) amplitude of density perturbation, and (c) nonlinear phase shift, obtained from the numerical solution to equations (19a) and (19b). Parameters correspond to  $Q = 4.25$ , and  $R = 1.32 \times 10^{-4}$ . The electron inertia length is set to zero.

ized to  $t_{\text{sat}}$ . Figure 1b shows the excited density perturbation that is driven by the ponderomotive force of the excited SAW. Note that as time proceeds, the magnetic field and density perturbation are constricted into a channel that becomes increasingly more narrow with time. The earthward edge of this channel stays at a more or less fixed  $x$ -position, while the resonance peak shifts slightly earthward (equatorward) with time. Figure 2 shows a cut along the  $x$  direction of Figure 1 at a time near  $4t_{\text{sat}}$ . In Figure 2b, the local decrease in density means that the resonance position, defined as the position  $x_c$  where  $\omega = k_z V_a(x)$ , moves to higher values of  $x$ . An analysis of equations (19a) and (19b)

shows that the resonance position cannot shift significantly beyond the first minimum in the magnetic field (near  $x = 0.6$  in Figure 2a). Narrowing therefore takes place asymmetrically, and in the absence of significant thermal pressure, the resonance width can become particularly narrow,  $\delta x \approx L\sqrt{\beta\gamma}$  in the strongly nonlinear case. If the plasma  $\beta$  is very small, nonlinear effects may cause the width of the FLR to become comparable to the electron inertial length, a regime we shall discuss later.

Figure 3 shows the temporal behavior of the wave field and density perturbation at two locations along  $x$ , namely,  $x = 0.5$ , and in the vicinity of the magnetic field maximum ( $x = 0.58$ ) in Figure 1. This figure shows that the SAW magnetic field saturates at the instant when the density perturbation goes through a minimum. Figure 3c shows the temporal nonlinear phase shift between the driver and the excited SAW at the position  $x = 0.5$ . Ponderomotive saturation of the SAW magnetic field occurs due to the temporal nonlinear frequency shift,  $\omega n/4$ , in equation (19a). Physically, this effect is the result of the ponderomotive force creating a nonuniform distribution of plasma along geomagnetic field lines. Note that the integrated mass density along each flux tube remains constant. However, the redistribution of plasma causes a decrease in the natural frequency of the magnetic field line with time. Once the nonlinear phase shift associated with this effect has reached  $\pi/2$ , the driver and locally excited SAW get out of phase and momentarily do not interact. When the instantaneous amplitude of the density perturbation returns through its minimum, the excited magnetic field can once again become reinforced by the driver. However, the earthward shift and narrowing of the resonance means that the peak value of the SAW magnetic field will move slightly earthward. The faint lines in Figures 3a and 3b correspond to temporal fluctuations of  $n$  and  $b$  near to the shifted resonance position, where the linear frequency detuning parameter  $\Delta\omega$  is nonzero. This contributes to the more rapid temporal growth that is seen near  $t = 5t_{\text{sat}}$ . At this time, the ponderomotive force has led to a near discontinuity in the density in the radial direction. Because dissipation and electron inertia are absent from this example, the resonance continues to narrow asymmetrically, and ultimately either of these two effects will be required to prevent further narrowing of the resonance.

For completeness, Figure 4 shows results for a warm plasma, satisfying  $Q = 12.25$  and  $R = 1.32 \times 10^{-4}$ . In this case, the increased thermal pressure prevents strong perturbations of the density. The maximum density perturbation is only 3% or so of the ambient density by the time  $t = 7t_{\text{sat}}$ , and differences between this warm plasma case and the results shown in Figure 3a are apparent. In particular, the asymmetrical shift of the SAW magnetic field peak amplitude occurs much later in time, after the resonance has grown to large amplitude. The maximum amplitude of the excited SAW magnetic field in Figure 4 is roughly a factor of 2 larger than in Figure 3a, and is determined by equation (24) rather than by equation (25). However, in spite of the

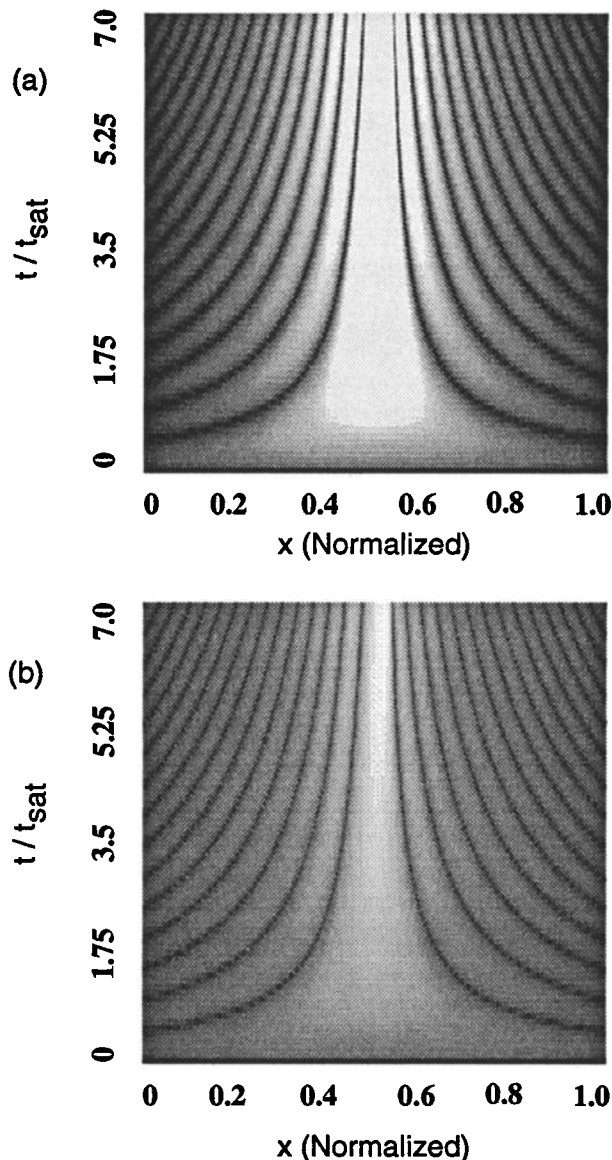


**Figure 4.** Temporal behavior of magnetic field amplitude obtained from the numerical solution to equations (19a) and (19b). Parameters correspond to  $Q = 12.25$  and  $R = 1.32 \times 10^{-4}$ . The electron inertia length is set to zero.

relatively small density fluctuations in this example, the temporal ponderomotive nonlinear phase shift that develops still leads to saturation of the wave fields.

In a warm plasma, the ponderomotive saturation amplitude is large, and correspondingly, the resonance is very narrow. In a cold plasma, the asymmetrical shift and extreme narrowing of the resonance can occur early in time, and both of these examples suggest that at some point nonideal MHD effects must be considered. If dissipation is small, the first modification that occurs is due to electron inertia. This is illustrated in Figure 5, which uses parameters of Figure 4, with  $Q = 12.25$ ,  $R = 1.32 \times 10^{-4}$ , and the electron inertia length finite and chosen such that the  $x$  dimension is  $400\lambda_e$ , where  $\lambda_e$  is the electron inertia length. Figure 5a shows the real and imaginary parts of the SAW magnetic field and

demonstrates that the finite group velocity of the SAW enables the wave to propagate earthward of the turning point. Figure 5b shows the amplitude of the SAW magnetic field and provides a comparison with results obtained by setting  $\lambda_e$  to zero. With finite electron inertia, the amplitude saturates at a lower level because of the earthward directed poynting flux. The maximum amplitude also shifts earthward after the wave fields have narrowed to several electron inertia lengths, in agreement with equation (9). Note that in this example, the electron inertial length is selected such that the resonance width at saturation is larger than for the ponderomotive mechanism.

Now we briefly consider electron inertia effects in a cold plasma for which the nonlinear parameter  $Q = 1.5$ . Figure 6 shows the amplitude of the real part of the SAW magnetic field and nonlinear density perturbations as a function of the  $x$  coordinate and time. The initial development up to time  $2t_{\text{sat}}$  is similar to the behavior observed with the electron inertia length set to zero. One significant difference is that the modification of the Alfvén speed profile by the ponderomotive force leads to earthward (equatorward) motion of the resonance position at the perpendicular group velocity

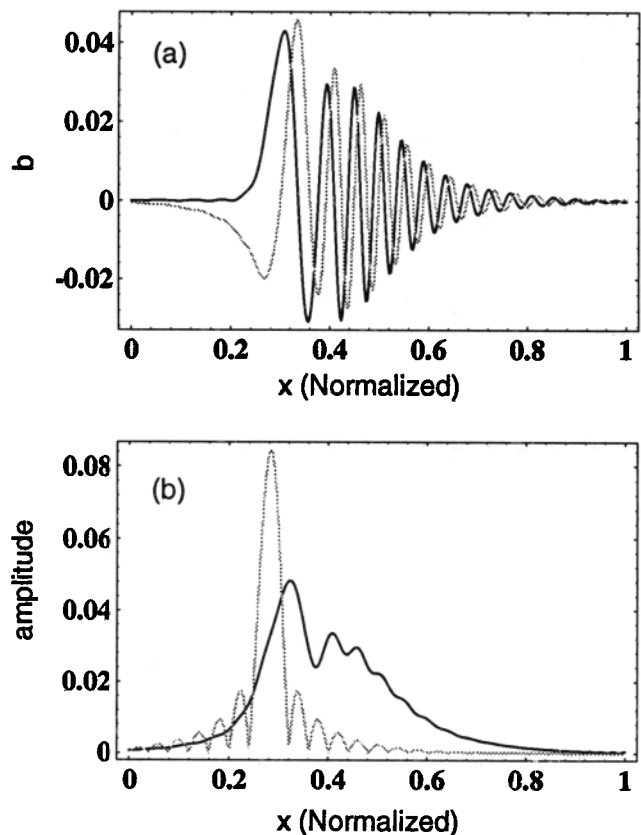


**Figure 5.** Shear Alfvén wave magnetic field near the time  $4t_{\text{sat}}$ . In Figure 5a the real part (bold line) and the imaginary part (faint line) of the magnetic field are sketched for the case where the  $x$  dimension is  $400\lambda_e$ . In Figure 5b the amplitude for the electron inertia case (bold line) is compared with the case for which  $\lambda_e = 0$  (faint line). Other parameters correspond to  $Q = 12.25$ .

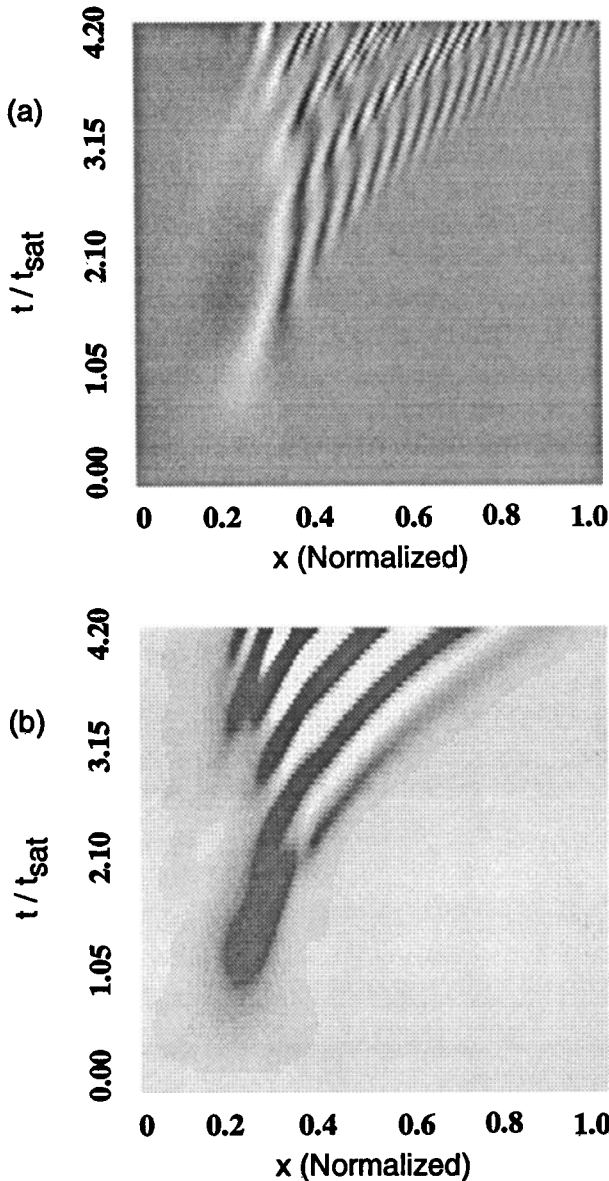


**Figure 6.** Temporal behavior of magnetic field amplitude and density perturbation obtained from the numerical solution to Equations (19a) and (19b). The nonlinear parameter  $Q = 1.5$ , and the  $x$  dimension is  $400\lambda_e$ .

of the electron inertia SAW. This is shown in Figure 7a, which shows the real part of  $b$  at times equal to  $1.2t_{\text{sat}}$  and  $2.4t_{\text{sat}}$ , respectively. Later in time, Figures 6 and 7b indicate that a transition stage occurs which involves a new set of spatial and temporal scales. We shall return to an explanation of this later.

## 7. Results of Three-Dimensional Numerical Simulations

In this section, we shall investigate the validity of the results described above by using a fully nonlinear 3-D computer model that solves the complete set of MHD equations (1)-(5). Our computer model imposes

periodic boundary conditions in the azimuthal  $y$  and field-aligned  $z$  directions, and in the direction of inhomogeneity  $x$ , we apply a reflecting boundary condition at  $x = L_x$ . At  $x = 0$ , we propagate into the system a monochromatic fast mode wave which reflects from its turning point near to the center of the inhomogeneity direction. Part of the fast mode energy evanescently tunnels to the resonant layer where it excites a SAW FLR. The remaining part of the fast mode energy reflects from the turning point and is able to freely exit through the  $x = 0$  boundary. Note that the  $x = 0$  boundary conditions involve using the fast mode dispersion relation  $\omega = \omega(\mathbf{k})$  to relate wave quantities  $(\delta\rho, \mathbf{b}, \mathbf{v})$  at  $x = 0$  to an imposed electric field. Then, the boundary conditions for each wave quantity at  $x = 0$  are expressed in the form

$$\frac{\partial f}{\partial t} - v \frac{\partial f}{\partial x} = 2 \frac{\partial f_i}{\partial t}, \quad (26)$$

which enables outgoing waves to pass freely through the boundary. In the above equation,  $f$  represents any fast mode quantity,  $v$  is the fast mode phase velocity in the  $x$  direction, and  $f_i$  is a prescribed (ingoing) wave quantity at  $x = 0$ . Note the difference between the manner in which the SAW FLR is excited in the full

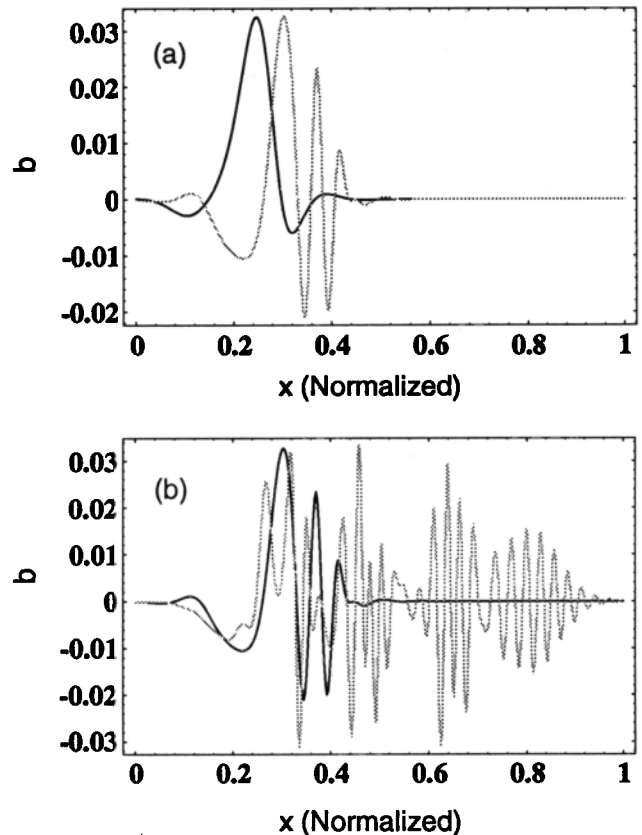


**Figure 7.** Temporal behavior of magnetic field amplitude obtained from the numerical solution to equations (19a) and (19b). In Figure 7a,  $t = 1.2t_{\text{sat}}$  (bold line) and  $t = 2.4t_{\text{sat}}$  (faint line). In Figure 7b  $t = 2.4t_{\text{sat}}$  (bold line) and  $t = 4t_{\text{sat}}$  (faint line). The nonlinear parameter  $Q = 1.5$ , and the  $x$  dimension is  $400\lambda_e$ .

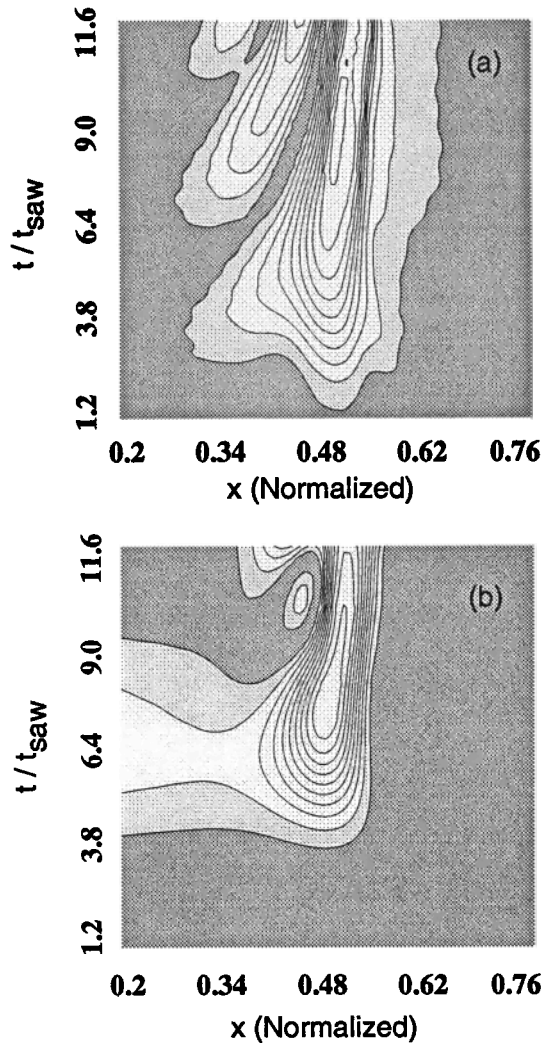


**Figure 8.** The temporal behavior of the amplitude of the (a) fundamental mode magnetic field and (b)  $2k_z$  component of the density perturbation from the numerical solution to equations (1)-(5). Parameters correspond to  $Q \approx 4.25$ . The maximum contour level in Figure 8a corresponds to  $0.13B_0$ , and in Figure 8b,  $\delta\rho = 0.33\rho_{\text{res}}$ , where  $\rho_{\text{res}}$  is the density at the resonance layer. The electron inertia length is set to zero.

nonlinear system and in the simplified model (equations (19a) and (19b)). In the latter, the driver is modeled by the constant term  $R$ , and nonlinear effects on the driver are therefore ignored. In the full system, the interaction of the fast mode driver and excited SAW is modeled self-consistently. In our simulations, we also impose an ambient magnetic field that is uniform along  $x$  so that the gradient in the Alfvén velocity is due to a spatially varying density profile.

In the following, we consider numerical solutions to the full set of MHD equations for different values of the nonlinear parameter  $Q$ . In the first case that is considered, for which  $Q \approx 4.25$ , we impose a flux of compressional Alfvén waves at the boundary of our system,  $x = 0$ , which gives a driver strength corresponding to  $R \approx 0.018$ . Figure 8 shows the Fourier ampli-

tudes (taking transforms in the  $y$  and  $z$  directions) of the  $y$  component of the fundamental mode ( $k_y, k_z$ ) of the SAW magnetic field and the ponderomotive force induced density perturbation ( $0, 2k_z$ ) as a function of  $x$  and time  $t$ , where the time axis is normalized to the number of wave periods of the incident fast mode driver. The localized nature of the excited SAW field and ponderomotive density perturbation is quite evident in this

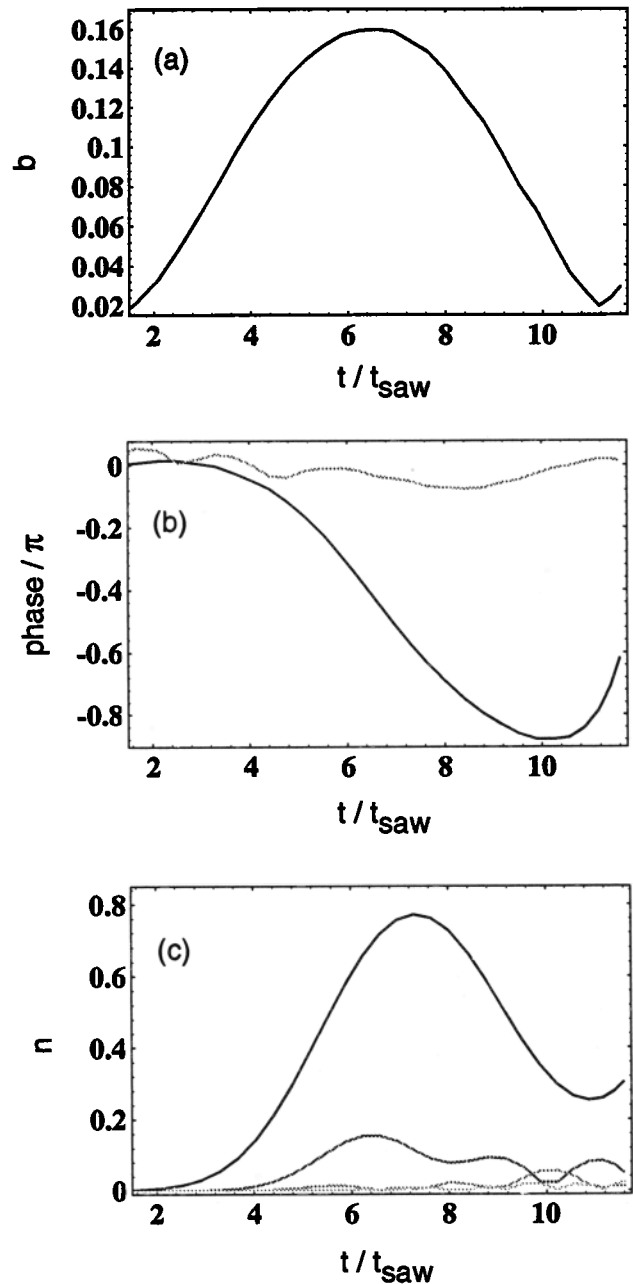


**Figure 9.** Temporal behavior of the amplitude of (a) the fundamental mode magnetic field, (b) nonlinear phase shift, and (c) ponderomotive density perturbation obtained from numerical solutions to equations (1)-(5). In Figure 9b, the bold line corresponds to Figure 9a, and the faint line is on a field line that is outside of the peak. In Figure 9b, the  $(0, 2k_z)$  spatial harmonic dominates higher modes. Parameters correspond to  $Q \approx 4.25$ .

figure. Figure 9 shows the nonlinear phase shift, density perturbation, and resulting local saturation of the wave fields of the excited SAW. On comparing Figures 9a and 9b, it can be seen that the SAW magnetic field saturates on a given field line when the ponderomotive nonlinear phase shift is approximately  $\pi/2$ . The faint horizontal line in Figure 9b shows the nonlinear phase shift that occurs on a field line which is outside of the FLR (to the right of the peak). It is clear that ponderomotive effects occur within the region of strong SAW fields. In Figure 9c we have also plotted the amplitude of  $(0, 2k_z)$  higher spatial harmonics of the density. These can be seen as the low-amplitude modes in Figure 9c, where it is clear that the lowest wavenumber mode  $(0, 2k_z)$  dominates over higher spatial harmonics. This confirms that our simplified model of FLRs derived earlier provides a valid description of the nonlinear dynamics in this example.

The time dependence of the  $b_z$  component of the compressional wave magnetic field is shown in Figure 10. This component of the magnetic field represents the driver term in the simplified model of FLR excitation discussed above. It can be seen that  $b_z$  is nearly constant across the resonance layer (from  $x = 0.4$  to  $x = 0.6$ ) during the first few periods of the excited SAW. However, after nonlinear effects become important,  $b_z$  becomes spatially inhomogeneous in a narrow region surrounding the resonance layer. At the time of nonlinear saturation, the spatially averaged driver strength in the vicinity of the resonance layer corresponds to  $R \approx 0.018$ . According to equation (25), the nonlinear saturation timescale is approximately 4.8 wave periods, and the saturated amplitude of the  $y$  component of the SAW magnetic field is predicted to be approximately  $0.18B_0$ . These estimates are found to be in good agreement with the numerical results shown in Figure 8. Subtracting the 2 Alfvén period linear ramp up time of the compressional wave field, Figure 9 shows that near the center of the magnetic field structure, nonlinear saturation occurs in approximately 4.6 periods, again in good agreement with the theory.

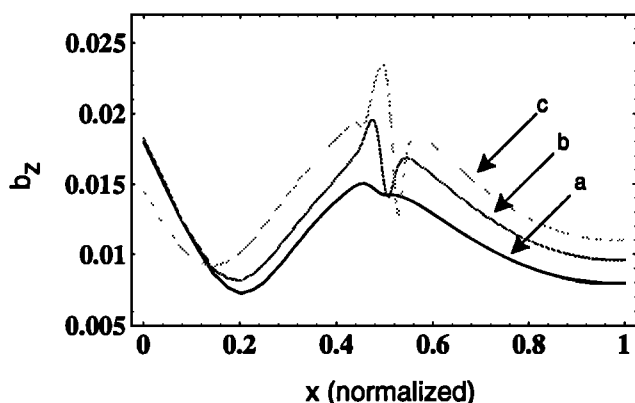


Figure 10. Temporal behavior of the amplitude of the  $b_z$  component of the fundamental mode magnetic field obtained from numerical solutions to equations (1)-(5). Parameters correspond to those of Figure (8). Curves labeled a-c correspond to time  $t = 3.9t_{\text{SAW}}$ ,  $t = 6.8t_{\text{SAW}}$ , and  $t = 11t_{\text{SAW}}$ , respectively.

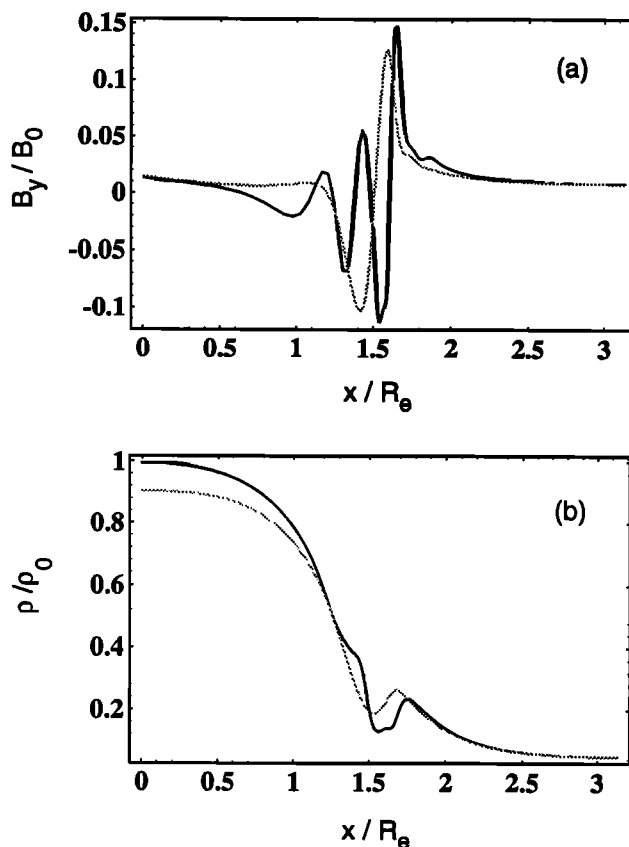


Figure 11. Radial dependence of (a) the  $B_y$  component of the magnetic field and (b) the plasma density obtained from numerical solutions to equations (1)-(5). The faint lines correspond to  $t = 6.8t_{\text{SAW}}$ , and the bold lines to  $t = 11t_{\text{SAW}}$ . Other parameters correspond to those of Figure 8.

Figure 11 shows the  $y$  component of the magnetic field and plasma density at one particular azimuthal position in the equatorial plane of the magnetosphere. Note that the  $x$ -axis scale is now plotted in terms of the real spatial coordinate. The faint lines show results near the time of nonlinear saturation, and the solid lines correspond to  $t \approx 11t_{\text{SAW}}$ . Figure 11b shows the modification to the plasma density that occurs as a result of the ponderomotive force of the excited SAW. The fluctuation in density near  $x = 0$  is due to the incident compressional wave. In Figure 11a, a slight earthward shift of the SAW magnetic field with time can be seen. It can also be observed that following the time of nonlinear saturation, the radial scale size of the resonance is quite narrow. Our simplified model equations indicate that following the time of ponderomotive saturation, nonlinear structuring can lead to radial scale sizes that are an order of magnitude smaller than for dissipative saturation. Unfortunately, in our 3-D model the spatial resolution of the finite difference grid prevents us from following the development of the FLR beyond the time indicated in Figure 11.

In terms of physical quantities, the minimum radial scale sizes reached in Figure 11 are of the order of  $0.1 R_E$ , with the overall width of the FLR being ap-

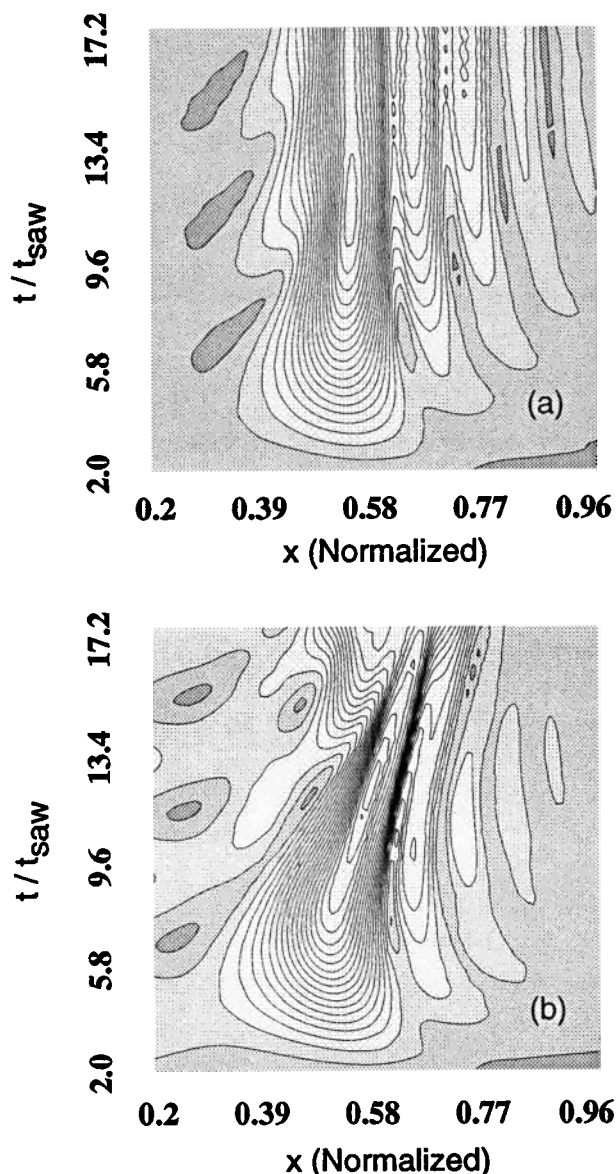


Figure 12. Temporal behavior of the amplitude of the fundamental mode magnetic field. Shown are (a) warm plasma with  $Q = 24$  and (b) cold plasma with  $Q \approx 1.5$ . In both cases, the electron inertia length is finite.

proximately  $1 R_E$ . Taking account of mapping factors between the equatorial plane and the ionosphere, the smallest scale size corresponds to a few kilometers above the ionosphere and is compatible with latitudinal scale sizes of FLRs observed in the  $F$  region [Samson *et al.*, 1992]. In the equatorial plane, Figure 11 also suggests that gyroradius effects might play an important role in the evolution of FLRs, with electron inertia effects becoming more important in the auroral accelerator region where the electron inertia length can be of the order of 1-2 km. We again caution that the limiting scale size in Figure 11 is set by the dissipation scale size of our numerical scheme. In reality, this limiting scale size is likely to be much smaller, and thus our results suggest that nonlinear radial structuring of FLRs may become significant.

Finally, we consider nonlinear ponderomotive effects in the presence of finite electron inertia. Figure 12 compares warm and cold plasma effects. In Figure 12a, ponderomotive effects are negligible, while in Figure 12b, parameters are chosen such that  $Q$  is approximately 1.5 at the resonance position. It is seen that ponderomotive effects lead to a significant motion of the FLR across the spatial gradient in the Alfvén speed profile and that narrowing of the resonance occurs as it shifts position. The results in Figure 12b also show that ponderomotive steepening of the Alfvén speed profile, which is very similar to that observed in Figure 11, leads to a truncated Airy-like pattern of the SAW magnetic field. This is more clearly seen in Figure 13, which shows cuts of the data in Figure 12 at times corresponding to  $t = 6t_{\text{SAW}}$  and  $t = 12t_{\text{SAW}}$ , respectively. This results from the fact that mode conversion is now taking place in a steepened Alfvén speed profile, with a correspondingly narrower resonance width. Note that the results shown in Figure 13b are in agreement with the behavior observed in Figure 7a, which was obtained using the reduced MHD models described earlier. The truncation of the spatial wave train in Figure 13b may explain why undamped Airy pattern signatures of FLRs are not easily observed.

The time development following  $t \approx 12t_{\text{SAW}}$  in Figure 12b differs significantly from that shown in Figure 7b. In the full MHD solutions, further nonlinear steep-

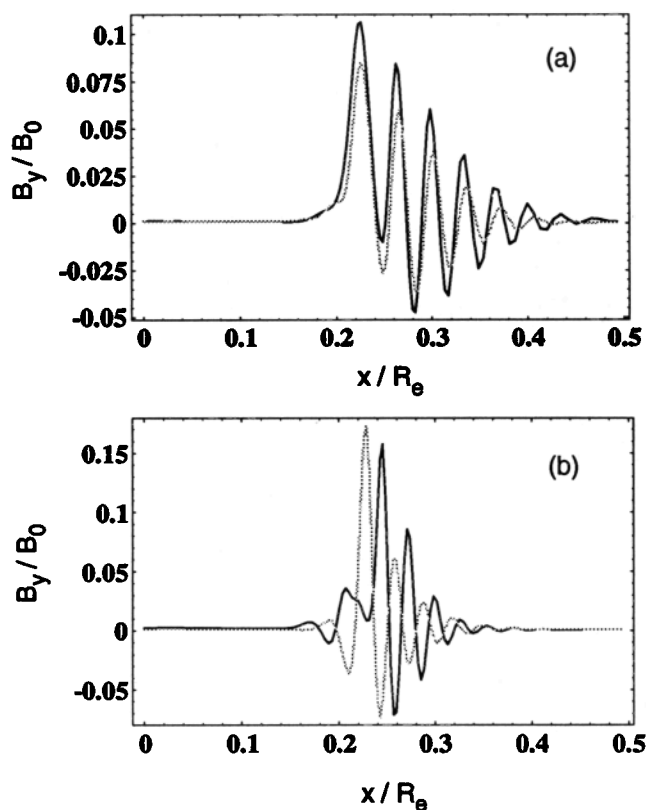


Figure 13. Spatial dependence of the fundamental mode magnetic field at  $t = 6t_{\text{SAW}}$  (faint lines) and  $t = 12t_{\text{SAW}}$  (bold lines). Shown are (a) warm plasma with  $Q = 24$  and, (b) cold plasma with  $Q \approx 1.5$ . In both cases, the electron inertia length is finite.

ening of the wave packet is prevented by the dissipation present in the numerical scheme, while in the reduced MHD model, a transition stage is observed, as discussed previously. An analysis shows that the transition observed in the reduced model, i.e., Figure 7b, is due to a secondary nonlinear process called the parametric decay instability [Galeev and Oraevskii, 1963]. This involves the decay of the SAW into a slow magnetosonic wave and a pair of daughter electron inertia SAWs. The dispersion associated with electron inertia SAWs means that frequency and wavenumber matching conditions can be satisfied for the decay instability provided the electron inertia length is finite. The growth rate for the decay process is exponential, and this introduces new temporal and spatial scales into the problem. This is beyond the scope of the present analysis and will be discussed in a separate publication.

## 8. Conclusions

We have presented theory and numerical simulations of highly nonlinear plasma processes associated with the ponderomotive force of standing shear Alfvén FLRs in a box model magnetosphere. The ponderomotive force drives nonlinear density perturbations which evolve as slow mode acoustic waves. The excited slow modes change the natural frequency of the magnetic field lines on which they are excited, and it has been shown that this can lead to nonlinear saturation of electron inertia SAWs that are being resonantly excited by compressional MHD fast mode waves. Using a simplified set of reduced MHD equations, we have derived expressions for the amplitude, width, and timescale of ponderomotive saturation and have shown that in low- $\beta$  plasma, the ponderomotive nonlinearity is the controlling factor in determining the temporal evolution of FLRs.

In the limit of vanishing electron inertia, ponderomotive saturation is accompanied by an asymmetrical narrowing and nonlinear radial structuring of the excited SAWs. With finite electron inertia, the asymmetrical narrowing and structuring of the FLR wave form coincides with earthward (equatorward) motion. This arises due to the perpendicular group velocity of electron inertia SAWs. When ponderomotive effects are dominant, the nonlinear steepening of the Alfvén speed profile confines the excited wave field to a narrow region, so that the spatial radial profile resembles a truncated Airy function. The plasma excavated by the ponderomotive force leads to the formation of a density cavity. Such cavities have been observed in the auroral zone. Ponderomotive saturation of FLRs is accompanied by a parametric decay of the excited electron inertia SAWs. The parametric decay evolves as a secondary process in the nonlinear evolution and introduces a new set of spatial and temporal scales that is currently under investigation. Fully nonlinear 3-D Cartesian simulation results have also been presented. The simulations have confirmed the main findings associated with the reduced MHD models.

Finally, it is interesting to compare the level of ponderomotive saturation of FLRs with another nonlinear

process: the Kelvin-Helmholtz (KH) instability. It is well known that the KH instability of a plasma shear flow has a maximum growth rate given approximately by  $\gamma_{KH} \approx 0.3V_y/a$ , where  $a$  is the thickness of the shear layer. In the case of FLRs, the thickness of the shear layer corresponds to  $a \approx \delta x/2 \approx 2\pi L/\omega t$ , and  $V_y$  can be related to the amplitude of the magnetic field  $b_y$  according to  $V_y \sim \omega b_y/B_0 k_z \approx R\omega^2 t/2k_z$  so that  $\gamma_{KH} \sim 0.024R\omega^3 t^2/k_z L$ . It is expected that the KH instability will only affect the resonance if it can develop during one period of the compressional Alfvén wave. Therefore we may roughly estimate  $\gamma_{KH} \approx \omega$  as the condition for FLR saturation due to the KH instability [Samson and Rankin, 1994] and arrive at  $b_{y,sat} \approx 3.2B_0\sqrt{k_z L R}$  and  $t_{sat} \approx 6.5\omega^{-1}\sqrt{k_z L/R}$ . The comparison of the timescales for saturation of the FLR by the KH instability and by the ponderomotive mechanism (equation (25)) demonstrates explicitly that the competition between these two nonlinear mechanisms, at least in the case of cold plasma,  $\beta \ll 1$ , depends on the relationship between the driver strength  $R$  and the plasma inhomogeneity scale  $k_z L$ . The ponderomotive nonlinearity develops faster and saturates at a lower level if  $R < (k_z L)^5$ . Our initial assumptions of weak plasma inhomogeneity,  $k_z L \gg 1$ , and weak driver,  $R \ll 1$ , favor the ponderomotive nonlinearity. However, it may not be so under realistic magnetospheric conditions because the parameter  $k_z L$  may be less than one and an increase of the plasma thermal pressure will lengthen the ponderomotive saturation time. We also cannot exclude the possibility that the KH instability will develop as a secondary instability of a ponderomotively saturated FLR.

**Acknowledgments.** Research for this project has been supported through the Canadian Space Agency, the Natural Sciences and Engineering Research Council of Canada, and in part by the Russian Foundation of Fundamental Investigations.

The Editor thanks W. J. Hughes, T. K. Nakamura, and two other referees for their assistance in evaluating this paper.

## References

- Allan, W., Plasma energization by the ponderomotive force of magnetospheric standing Alfvén waves, *J. Geophys. Res.*, **98**, 11,383, 1993.
- Allan, W., and E. M. Poulter, ULF waves - Their relationship to the structure of the Earth's magnetosphere, *Rep. Prog. Phys.*, **55**, 533, 1992.
- Boehm, M. H., C. W. Carlson, J. P. McFadden, J. H. Clemmons, and F. S. Moze, High resolution sounding rocket observations of large-amplitude Alfvén waves, *J. Geophys. Res.*, **95**, 12,157, 1990.
- Borovsky, J. E., Auroral arc thickness as predicted by various theories, *J. Geophys. Res.*, **98**, 6101, 1993.
- Chen, L., and A. Hasegawa, A theory of long period magnetic pulsations, 1, Steady excitation of field line resonances, *J. Geophys. Res.*, **79**, 1024, 1974.
- Cummings, W. D., R. J. O'Sullivan, and P. J. Coleman Jr., Standing Alfvén waves in the magnetosphere, *J. Geophys. Res.*, **74**, 778, 1969.
- Fenrich, F. R., J. C. Samson, G. Sofko, and R. A. Greenwald,

- ULF high- and low- $m$  field line resonances observed with Super Dual Auroral Radar Network, *J. Geophys. Res.*, **100**, 21,535, 1995.
- Forslund, D. W., J. M. Kindel, K. Lee, E. L. Lindman, and R. L. Morse, Theory and simulation of absorption in a hot plasma, *Phys. Rev. A*, **11**, 679, 1975.
- Galeev, A. A., and V. N. Oraevskii, The stability of Alfvén waves, *Sov. Phys. Dokl., Engl. Transl.*, **7**, 988, 1963.
- Goertz, C. K., Kinetic Alfvén wave on auroral field lines, *Planet. Space Sci.*, **32**, 1387, 1984.
- Greenwald, R. A., and A. D. M. Walker, Energetics of long period resonant hydromagnetic waves, *Geophys. Res. Lett.*, **7**, 745, 1980.
- Kivelson, M. G., and D. J. Southwood, Resonant ULF waves: A new interpretation, *Geophys. Res. Lett.*, **12**, 49, 1985.
- Kivelson, M. G., and D. J. Southwood, Coupling of global magnetospheric MHD eigenmode to field line resonances, *J. Geophys. Res.*, **91**, 4345, 1986.
- Lee, D. H., and R. L. Lysak, Magnetospheric ULF wave coupling in the dipole model: The impulsive excitation, *J. Geophys. Res.*, **94**, 17,097, 1989.
- Lee, L. C., and C. Q. Wei, Interaction of the solar wind with the magnetopause boundary layer and generation of magnetic impulse events, *J. Atmos. Sol. Terr. Phys.*, **55**, 967, 1993.
- Li, X., and M. Temerin, Ponderomotive effects on ion acceleration in the auroral zone, *Geophys. Res. Lett.*, **20**, 13, 1993.
- Mozer, F. S., The low altitude electric field structure of discrete auroral arcs, in *Physics of Auroral Arc Formation*, *Geophys. Monogr. Ser.*, vol. 25, edited by S.-I. Akasofu and J. R. Kan, pp. 136-142, AGU, Washington, D.C., 1981.
- Rankin, R., B. G. Harrold, J. C. Samson, and P. Frycz, The nonlinear evolution of field line resonances in the Earth's magnetosphere, *J. Geophys. Res.*, **98**, 5839, 1993a.
- Rankin, R., J. C. Samson, and P. Frycz, Simulations of driven field line resonances in the Earth's magnetosphere, *J. Geophys. Res.*, **98**, 21,341, 1993b.
- Rankin, R., P. Frycz, V. T. Tikhonchuk, and J. Samson, Nonlinear standing shear Alfvén waves in the Earth's magnetosphere, *J. Geophys. Res.*, **99**, 21,291, 1994.
- Rankin, R., P. Frycz, V. T. Tikhonchuk, and J. C. Samson, Ponderomotive saturation of magnetospheric field line resonances, *Geophys. Res. Lett.*, **22**, 1741, 1995.
- Ruohoniemi, J. M., R. A. Greenwald, K. B. Baker, and J. C. Samson, HF radar observations of Pc5 field line resonances in the midnight/early morning MLT sector, *J. Geophys. Res.*, **96**, 15,697, 1991.
- Samson, J. C., Three-dimensional polarization characteristics of high latitude Pc5 geomagnetic micropulsations, *J. Geophys. Res.*, **77**, 6145, 1972.
- Samson, J. C., and R. Rankin, The coupling of solar energy to MHD cavity modes, waveguide modes, and field line resonances in the Earth's magnetosphere, in *Solar Wind Sources of Magnetospheric Ultra-Low-Frequency Waves*, *Geophys. Monogr. Ser.*, vol. 81, edited by M. J. Engebretson, K. Takahashi, and M. Scholer, pp. 253-264, AGU, Washington, D.C., 1994.
- Samson, J. C., T. J. Hughes, F. Creutzberg, D. D. Wallis, R. A. Greenwald, and J. M. Ruohoniemi, Observations of a discrete arc in association with field line resonances, *J. Geophys. Res.*, **96**, 15,683, 1991.
- Samson, J. C., D. D. Wallis, T. J. Hughes, F. Creutzberg, J. M. Ruohoniemi, and R. A. Greenwald, Substorm intensifications and field line resonances in the nightside magnetosphere, *J. Geophys. Res.*, **97**, 8495, 1992.
- Samson, J. C., L. L. Cogger, and Q. Pao, Observations of field line resonances, auroral arcs, and auroral vortex structures, *J. Geophys. Res.*, **101**, 17,373, 1996a.
- Samson, J. C., R. Rankin, P. Frycz, V. Tikhonchuk, and L. L. Cogger, Ultra low frequency field line resonances and auroral arcs, in *Physics of Space Plasmas*, **14**, edited by T. Chang and J. R. Jasperse, p. 457, MIT Cent. for Theor. Geo/Cosmo Plasma Phys., Boston, Mass., 1996b.
- Southwood, D. J., Some features of field line resonances in the magnetosphere, *Planet. Space Sci.*, **22**, 483, 1974.
- Southwood, D. J., and W. J. Hughes, Theory of hydromagnetic waves in the magnetosphere, *Space. Sci. Rev.*, **35**, 301, 1983.
- Speziale, T., and P. J. Catto, Linear wave conversion in an unmagnetized, collisionless plasma, *Phys. Fluids*, **20**, 990, 1977.
- Streltsov, A., and W. Lotko, The fine structure of dispersive, nonradiative field line resonance layers, *J. Geophys. Res.*, **100**, 19,457, 1995.
- Tikhonchuk, V. T., R. Rankin, P. Frycz, and J. C. Samson, Nonlinear dynamics of standing shear Alfvén waves, *Phys. Plasmas*, **2**, 501, 1995.
- Walker, A. D. M., J. M. Ruohoniemi, K. B. Baker, R. A. Greenwald, and J. C. Samson, Spatial and temporal behavior of ULF pulsations observed by the Goose Bay HF radar, *J. Geophys. Res.*, **97**, 12,187, 1992.
- Wei, C. Q., J. C. Samson, R. Rankin, and P. Frycz, Electron inertial effects on geomagnetic field line resonances, *J. Geophys. Res.*, **99**, 11,265, 1994.
- Weimer, D. R., and D. A. Gurnett, Large-amplitude auroral electric fields measured with DE 1, *J. Geophys. Res.*, **98**, 13,557, 1993.
- Xu, B. L., J. C. Samson, W. W. Liu, F. Creutzberg, and T. J. Hughes, Observations of optical aurora modulated by resonant Alfvén waves, *J. Geophys. Res.*, **98**, 11,531, 1993.
- Yumoto, K., External and internal sources of low frequency MHD waves in the magnetosphere: A review, *J. Geomagn. Geoelectr.*, **40**, 293, 1988.
- Zhu, X. and M. G. Kivelson, Analytic formulation and quantitative solutions of the coupled ULF wave problem, *J. Geophys. Res.*, **93**, 8602, 1988.
- Ziesolleck, C. W. S., and D. R. McDiarmid, Auroral latitude Pc5 field line resonances: Quantized frequencies, spatial characteristics, and diurnal variation, *J. Geophys. Res.*, **99**, 5817, 1994.

R. Rankin, Physics Department, University of Alberta, Edmonton, Alberta, Canada T6G 2J1. (e-mail: rankin@space.ualberta.ca)

V. T. Tikhonchuk, P. N. Lebedev Physics Institute, Russian Academy of Sciences, Moscow, 117924, Russia.

(Received August 11, 1997; revised October 27, 1997; accepted April 10, 1998.)